Acta Cryst. (1980). B**36**, 1355–1367

Second-Order Phase Transition of 1,4-Butanediyldiammonium Manganese Tetrachloride. A Neutron Diffraction Study on Clustered Crystals

BY K. TICHÝ AND J. BENEŠ

Institut für Reaktortechnik, Eidgenössische Technische Hochschule Zürich, CH-5303 Würenlingen, Switzerland

AND R. KIND AND H. AREND

Laboratorium für Festkörperphysik, Eidgenössische Technische Hochschule, CH-8093 Zürich, Switzerland

(*Received* 25 *January* 1979; *accepted* 14 *January* 1980)

Abstract

At $T = 295$ K, 1,4-butanediyldiammonium manganese tetrachloride, $NH_3(CH_2)_4NH_3MnCl_4$, is monoclinic, space group $P2_1/b$ with $Z = 2$ and unit-cell parameters $a = 10{\cdot}770\ (5)$, $b = 7{\cdot}177\ (3)$, $c = 7{\cdot}307\ (3)$ Å and $\gamma = 92{\cdot}67\ (5)°$. A second-order phase transition takes place at 382 ± 1 K. A high-temperature phase (measured at $T = 404 \pm 3$ K) is orthorhombic, space group *Pnmb* with $Z = 2$ and $a = 10{\cdot}690\ (5)$, $b = 7{\cdot}218\ (4)$, $c = 7{\cdot}337\ (3)$ Å. The sample used for neutron diffraction was clustered; it contained four single-crystal individuals at 295 K and three individuals at 404 K. Full-matrix least-squares refinement yielded $R(F) = 0{\cdot}1587$ and $R_w(F) = 0{\cdot}0668$ for 1579 resolved reflections at 295 K and $R(F) = 0{\cdot}1814$ and $R_w(F) = 0{\cdot}0704$ for 1337 resolved reflections at 404 K. Both structures consist of parallel two-dimensional sheets of puckered perovskite-type layers of corner-sharing $MnCl_6$ octahedra, interleaved by layers of 1,4-butanediyldiammonium chains nearly perpendicular to the layers. At 295 K, an almost planar chain subtends an angle of 38° with the *ac* plane. Ammonium groups at the ends of the chains fit into cavities of adjacent $MnCl_4$ layers and form N–H···Cl hydrogen bonds. Each in-plane Cl atom binds one H atom only [H···Cl = 2·316 (13) Å], while out-of-plane Cl atoms are linked by two hydrogen bridges [2·282 (12) and 2·428 (15) Å] to two neighbouring organic chains. At room temperature, the organic chain is ordered. Near the transition to the high-temperature phase, a dynamical disorder of the chains between two possible orientations, which becomes symmetric at the transition temperature, sets in. This results in the creation of a mirror plane $\{m_y|000\}$ which generates, together with the symmetry elements of the room-temperature phase $P2_1/b$, the high-temperature space group *Pnmb*. Organic ions occupy dynamically disordered positions related by the mirror plane. The angle subtended by projections of –C–N bonds into the *bc* plane is 77·3°. The ammonium H atom which forms the strongest hydrogen bond [2·328 (17) Å] to the out-of-plane Cl atom occupies the ordered position on the mirror plane; the other two ammonium H atoms are disordered and form one hydrogen bond [2·469 (38) Å] to the in-plane Cl atom and one hydrogen bond [2·699 (52) Å] to the out-of-plane Cl atom. The $MnCl_4$ layer, ordered in both phases, is two-dimensionally puckered at 295 K with Mn–Cl in-plane distances of 2·608 (5) and 2·574 (5) Å and with the out-of-plane distance 2·502 (4) Å. At 404 K the mirror plane constrains all Cl atoms into special positions and the puckering of the $MnCl_4$ layer along the *b* axis disappears. The one-dimensionally puckered layer contains only one in-plane Mn–Cl distance 2·615 (2) Å. The out-of-plane Mn–Cl distance is 2·511 (5) Å.

Introduction

1,4-Butanediyldiammonium manganese tetrachloride (subsequently abbreviated $BDAMnCl_4$) exhibits a second-order phase transition at 382 ± 1 K. This neutron diffraction study of the crystal structures above and below the transition temperature was performed at 404 and 295 K respectively and is a continuation of neutron diffraction investigations carried out in the series of chloride perovskite compounds of the general formula $NH_3(CH_2)_nNH_3MCl_4$, with M = Cu, Mn, Fe. In our preceding paper (Tichý, Beneš, Hälg & Arend, 1978) we described the room-temperature structures of substances with M = Cu, Mn and $n = 2$ (*i.e.* ethylenediammonium copper and manganese tetrachlorides, subsequently abbreviated $EDACuCl_4$ and $EDAMnCl_4$). Willett & Riedel (1975) published neutron work on substances with M = Fe, Mn and $n = 3$ and Walpen (1976) described the substances with M = Cd and $n = 2$–7. Some preliminary results on the title substance have been published elsewhere (Arend, Tichy, Baberschke & Rys, 1976).

0567-7408/80/061355-13$01.00

Experimental

$BDAMnCl_4$ was prepared in an aqueous solution by reaction of the metal chloride with 1,4-butanediyldiammonium dichloride according to the formula:

$$ClNH_3{-}(CH_2)_4{-}NH_3Cl + MnCl_2 \rightarrow [NH_3{-}(CH_2)_4{-}NH_3]MnCl_4.$$

This preparation is made possible by the congruent solubility of $BDAMnCl_4$. The solubility at 293 K is 0·0623 mol per mol H_2O with a positive temperature coefficient of 0·0177 K^{-1}.

Crystals were grown from the aqueous solution either by slow evaporation or by a temperature-gradient technique (Arend, Huber, Mischgofsky & Richter-van Leeuwen, 1978). The composition of the crystals was verified by volumetric analysis for Mn and Cl atoms. Crystals grow as thin transparent pale-yellowish plates. A non-deuterated sample used for neutron diffraction work was cut from a thicker plate grown by slow evaporation over a period of two months.

The structure analysis was undertaken on twinned samples because we did not succeed in growing untwinned crystals. The twinning is rather complicated; the sample contained four single-crystal individuals in the monoclinic room-temperature phase (subsequently abbreviated MRT), and the geometric relation of their reciprocal lattices is shown in Fig. 1. The individuals (1 and 3) and (2 and 4) are related by the same twinning law as for $EDAMnCl_4$; the pairs (1 and 2) and (3 and 4) are governed by the twinning law applicable for $EDACuCl_4$ (Tichý, Beneš, Hälg & Arend, 1978). The latter twinning law was not discovered until we centred orienting reflections on a four-circle neutron diffractometer, when we accidentally found a third reflection satellite from the reflection 040. The third individual was easily identified, but the fourth (here No. 2) was more difficult to find, because its reflections were rather weak as its volume amounted to only 8% of the total volume of the sample. The discovery that $BDAMnCl_4$ tends to be quadruplicated explains our previous incorrect determination of space-group extinctions (Arend, Tichý, Baberschke & Rys, 1976) ($hk0$: $k = 2n$ strong, $k = 2n + 1$ weak, but systematically and significantly present; $00l$: $l = 2n$) based on Weissenberg photographs taken from samples which were assumed to be only twinned. The weak reflections $hk0$, $k = 2n + 1$ are in fact the reflections $h0l$, $l = 2n + 1$ from second pairs of individuals and the correct space group of the room-temperature phase is therefore $P2_1/b$ (No. 14). The presence of the second twin in the small volume of the sample used for X-ray work indicates that the twinning is a very genuine feature of $BDAMnCl_4$.

We anticipated that the high-temperature phase would be orthorhombic (subsequently abbreviated OHT) and that two paired individuals (1 and 3) would merge into one [similarly the pair (2 and 4)], so that the OHT phase would contain two individuals only. However, three single-crystal individuals were found, two of them only slightly (~1°) misoriented. This can be explained by a strain imposed on the sample by straightening the monoclinic angle γ to 90° and this explanation is supported by a visible blemish which appeared on the sample after it was heated.

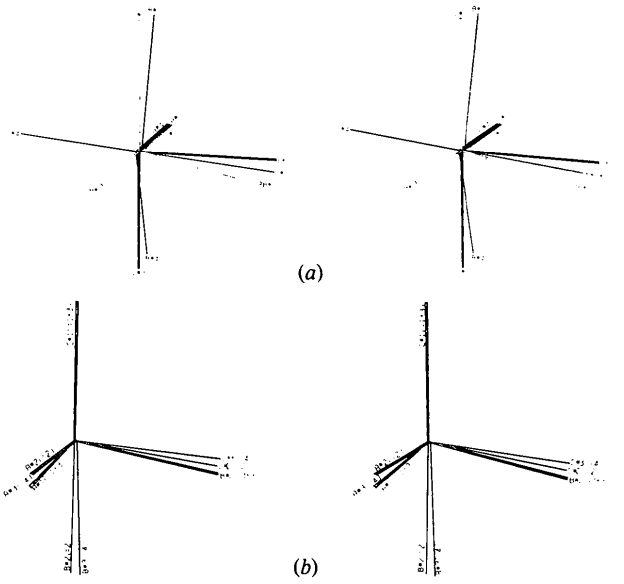

Fig. 1. Stereoviews (drawn with *ORTEP* II, Johnson, 1971) of the 'twinning' scheme of $BDAMnCl_4$. Reciprocal-lattice vectors are drawn with the serial number of the single-crystal individuals appended. (*a*) Room-temperature phase. The monoclinic angle γ is exaggereated 5×. (*b*) High-temperature phase. The misorientation of the reciprocal lattices is exaggerated about 7×. Serial numbers of room-temperature parental individuals are in parentheses.

In the OHT phase the indexing of orienting reflections and their assignments to three single-crystal individuals was rather troublesome because of a small misorientation of individuals 2 and 3, and was greatly facilitated by an iterative method and the computer program *ASSING*, published elsewhere (Tichý & Beneš, 1979).

Room-temperature unit-cell parameters were refined by a least-squares fit to Cu $K\bar{\alpha}$ powder data from ground crystals; the high-temperature ones were calculated by a least-squares method (Tichý, 1970) from 41 orienting reflections carefully centred on a four-circle neutron diffractometer. The neutron wavelength used (1·2932 Å) was calibrated by measuring $\Delta\theta = \theta(444) - \theta(111)$ from a Ge single-crystal slab [$d(111) = 3{\cdot}265$ Å].

Unit-cell parameters and space groups of both phases were verified by measuring reflections which should be systematically extinct according to space-

Table 1. *Crystal and experimental data for the room- and high-temperature phases of* 1,4-*butanediyldiammonium manganese tetrachloride*

	Room-temperature, $T = 295$ K	High-temperature phase, $T = 404$ K
Formula	$NH_3(CH_2)_4NH_3MnCl_4$	
Molecular weight	286·92	
Space group	Monoclinic, No. 14, $P2_1/b$; $hk0$, $k = 2n$ $00l$, $l = 2n$	Orthorhombic, No. 53, $Pnmb$; $0kl$, $k + l = 2n$ $hk0$, $k = 2n$
Temperature	295 ± 3 K	404 ± 3 K
Unit-cell dimensions	$a =$ 10·770 (5) Å	$a =$ 10·690 (5) Å
	$b =$ 7·177 (3)	$b =$ 7·218 (4)
	$c =$ 7·307 (3)	$c =$ 7·337 (3)
	$\gamma =$ 92·67 (5)°	
	$V = 564{\cdot}2$ (4) Å^3	$V = 566{\cdot}1$ (4) Å^3
Density	$D_{obs} = 1{\cdot}653$, $D_{calc} = 1{\cdot}689$ Mg m^{-3}	$D_{calc} = 1{\cdot}683$ Mg m^{-3}
Molecules per unit cell	2	2
Principal growth face	Plate parallel with (100)	
'Twinning'	Four individuals	Three individuals
indices of reflection satellites	hkl_1, $\bar{h}k\bar{l}_3$ → hkl_1	
	$\bar{h}lk_2$ → $h\bar{l}k_2$	
	$\bar{h}\bar{l}k_4$ → $h\bar{l}k_3$	
relative volumes of single-crystal individuals		
– based on scale factors	0·213, 0·081, 0·230, 0·476	0·483, 0·173, 0·344
– expected from room-temperature study	–	0·443, 0·081, 0·476
number of orienting reflections for establishing unit cell and orientation of individuals	16, 13, 16, 13 (32 altogether)	17, 13, 14 (41 altogether)
Data collection		
wavelength	1·0308 Å	1·2932 Å
monochromator	Pyrolytic graphite	Cu(111)
$\lambda/2$ contamination	~1%	7·9 ± 0·3%
scan length (°)	1·45 (0·44 + 2·26 tan θ)	(2·90 tan$^2\theta$ − 3·54 tan θ + 1·38)$^{1/2}$
scanning mode	ω:2θ, 40–60 points per reflection cluster	
monitor count	40 000	40 000; for sin $\theta/\lambda > 0{\cdot}45$ Å^{-1} 100 000
$(\sin\theta/\lambda)_{max}$	0·570 Å^{-1}	0·605 Å^{-1}
sample mounting	(100) plane parallel with the diffractometer φ axis	
reference reflections and their behaviour	$\bar{4}00_1 \equiv 400_2 \equiv 400_3 \equiv 400_4$, $00\bar{4}_1 \equiv 004_3$, $00\bar{4}_2 \equiv 004_4$, $0\bar{4}0_1$, $0\bar{4}0_2$, $0\bar{4}0_3$, 040_4	$900_2 + 900_3$, 040_1, $00\bar{4}_1$, $040_2 \equiv 040_3$, $004_2 \equiv 004_3$, 360_1, $306_2 + 306_3$.
	No significant variation	
interval between measurement of reference reflections	2–3 days	
Crystal sample and absorption corrections		
weight	24·83 mg	
volume	14·75 mm^3	
shape	Polyhedron, 3·5 × 3·0 × 1·4 mm	
number of boundary planes	6	
linear absorption coefficient μ (including incoherent scattering)	0·250 mm^{-1}	0·312 mm^{-1}
range of transmission factor	0·414–0·754	0·358–0·675
range of mean path length	0·01089–0·03519 mm	0·01214–0·03220 mm
Reflections		
number of reflections measured (excluding standard reflections)	1579	1509
number of symmetry-independent reflections for single-crystal individuals 1,2,3,4	225, 288, 309, 632	341, 334, 369
total number of independent reflections (regardless of individuals 1,2,3,4)	735	424
number of reflections missing (unmeasured or unresolved)	169	193
range of hkl	±11, ±8, ±8	±12, ±8, ±8
range of intensities (relative scale)	1–1043	1–992

group extinctions and with $\sin\theta/\lambda \leq 0{\cdot}19$ Å^{-1}, also reflections $h/2\ k/2\ l/2$. No violations were observed for the MRT phase. For the OHT phase there were four weak but significant reflections which disobeyed the law $hk0$, $k = 2n$ for systematic extinctions. Measurements of these reflections at different angles of rotation about the scattering vector showed that they were caused by multiple scattering.

The sample was heated by a broad (25 mm in diameter) stream of hot air which was blown on the sample along the diffractometer axis χ with a velocity of about 5 m s^{-1}. The hot-air stream was enclosed by a cylindrical cool-air stream 10 mm wide. Both streams were brought to the sample by two cylinders made from thin vanadium foil which were coaxial with the χ axis. A thermocouple mounted in the muzzle of the hot-air cylinder was used for the temperature measurement and control; the sample was 2 mm from this thermocouple. The volume of constant temperature was about 20 mm from the muzzle along the χ axis axially and from the χ axis about 10 mm radially. Short-term temperature fluctuations caused by the control circuit were less than ±2 K, the average long-term stability was better than 1 K. The thermocouple was calibrated by a laboratory mercury thermometer.

Measurements were performed at the reactors Diorit and Saphir of the Swiss Federal Institute for Reactor Research at Würenlingen. A novel method for measuring clustered crystals was used. By bringing the measured reciprocal vector and its nearest reflection satellite into the equatorial plane of a four-circle diffractometer, and by checking for interference from not-measured satellite reciprocal vectors, a maximum resolution of peaks was achieved (Beneš & Tichý, 1975; Tichý & Beneš, 1977). We succeeded in measuring about 80% of all independent reflections at room temperature; for the OHT phase, where the overlapping was more troublesome, we could measure only about 70% of all independent reflections.

Integrated intensities were derived from reflection profiles and their standard deviations $\sigma(I)$ from counting statistics. When reflections with unequal F_{calc} were so close that they partly overlapped, their $\sigma(I)$ values increased with increasing overlap. Intensities of unobserved reflections were given 50% of the 'threshold' of measureable intensity with $\sigma(I)$ of the same value and were included in the subsequent least-squares refinement. For the high-temperature data the corrections for attenuation of primary and diffracted beams in the vanadium heating cylinders were applied. The linear absorption coefficient μ of the sample was determined by a transmission of pinhole-collimated neutrons for $\lambda = 1{\cdot}0308$ Å through thicker crystal platelets; for $\lambda = 1{\cdot}2932$ Å, μ was computed from the $1/v$ law. Absorption corrections and mean path lengths (for extinction corrections) were computed with the assumption that four or three single-crystal individuals were evenly distributed over the whole volume of the sample. Crystal data and experimental details are summarized in Table 1.

Structure determination and refinement

Room-temperature phase (MRT)

$EDAMnCl_4$ (Tichý *et al.*, 1978) and $BDAMnCl_4$ crystallize in the same space group, they have very similar b and c axes and the difference in their a-axis lengths is just one $-CH_2-CH_2-$ zigzag distance of the organic chain. Therefore, the starting atomic coordinates for $BDAMnCl_4$ were derived from the structure of $EDAMnCl_4$ with its organic chains expanded by two CH_2 units.

Difficulties were encountered only in the initial stage of the refinement, where only four independent scale factors, an overall temperature factor and an extinction parameter r^* were refined with a reduced set of reflections in the range $\sin\theta/\lambda < 0{\cdot}30$ Å^{-1}. Once these six parameters were about right, the refinement proceeded smoothly. The isotropic secondary-extinction parameter r^* (Zachariasen, 1967) was included

Table 2. *Summary of the least-squares refinement*

The extinction coefficient y is defined (Zachariasen, 1967) as $F^2_{measured} = yF^2_{kinematical}$. $F_{corr} = F_{obs}/\sqrt{y}$ is the observed structure factor corrected for extinction.

	$BDAMnCl_4$ $T = 295$ K	$BDAMnCl_4$ $T = 404$ K
Number of parameters refined (n)	118	105
Number of observations, including zero intensities (m)	1579	1337
Number of independent reflections (m_1)	735	424
Number of scale factors		
total	10	6
independent	4	3
Ratio m_1/n	6·23	4·04
Final shift/e.s.d. ratio		
for scale factors	<0·3	<0·3
for xyz, non-H atoms	<0·1	<0·2
for xyz, H atoms	<0·2	<0·2
for b_{ij} of all atoms	<0·3	<0·4
$R(F) = \sum \lvert F_{corr} - \lvert F_{calc}\rvert\rvert / \sum F_{corr}$	0·1587	0·1814
$R_w(F) = [\sum w(F_{corr} - \lvert F_{calc}\rvert)^2 / \sum wF^2_{corr}]^{1/2}$	0·0668	0·0704
$S = [\sum w(F_{corr} - \lvert F_{calc}\rvert)^2/(m-n)]^{1/2}$	4·9090	4·7593
y for reflection 022 (most affected by extinction)	0·373	0·837
Extinction parameter r^* (isotropic, secondary only)	7067·2	668·0
Measured with neutron wavelength λ	1·0308 Å	1·2932 Å
Weighting scheme	$w = 1/\sigma^2(F)$ where $\sigma(F) \sim \sigma(I)\sqrt{I}$	
Refinement based on	F	
Function minimized	$\sum w(F_{corr} - \lvert F_{calc}\rvert)^2$	
Neutron scattering lengths used in refinement (fm)	$b_{Mn} = -3{\cdot}90$ $b_{Cl} = 9{\cdot}60$ $b_C = 6{\cdot}65$ $b_N = 9{\cdot}40$ $b_H = -3{\cdot}74$	

Table 3. *Positional parameters* ($\times 10^4$) *for the MRT and OHT phases of* $BDAMnCl_4$

E.s.d.'s in parentheses refer to the last significant figures.

MRT phase				OHT phase			
	x	*y*	*z*		*x*	*y*	*z*
Mn	0*	0*	0*	Mn	0*	0*	0*
Cl(1)	−224 (3)	2647 (6)	2380 (7)	Cl(1)	−205 (5)	2500*	2500*
Cl(2)	2289 (3)	285 (6)	446 (6)	Cl(2)	2301 (3)	0*	389 (7)
C(1)	3330 (5)	5545 (12)	−570 (11)	C(1)	3304 (10)	5343 (185)	−552 (20)
H(11)	3361 (12)	5320 (39)	−2001 (14)	H(11)	3362 (22)	4387 (57)	−1907 (26)
H(12)	3366 (13)	7072 (18)	−626 (31)	H(12)	3377 (31)	6968 (30)	−743 (92)
C(2)	4395 (5)	4736 (13)	410 (11)	C(2)	4401 (13)	4530 (24)	462 (26)
H(21)	4327 (13)	4868 (35)	1788 (20)	H(21)	4297 (32)	4271 (206)	1729 (45)
H(22)	4310 (11)	3225 (17)	441 (37)	H(22)	4424 (41)	3428 (133)	693 (100)
N	2117 (4)	4959 (9)	188 (8)	N	2105 (9)	4730 (58)	202 (21)
H(3)	2076 (12)	5235 (28)	1506 (16)	H(3)	2033 (13)	5000*	1549 (24)
H(4)	1390 (9)	5634 (18)	−467 (18)	H(4)	1473 (22)	5609 (68)	−530 (28)
H(5)	1974 (11)	3528 (19)	98 (29)	H(5)	1849 (49)	3594 (78)	316 (69)

* Parameters not refined (atoms in special positions).

in the full-matrix least-squares refinement with a modified version of the program *ORFLS* (Busing, Martin & Levy, 1962) on non-averaged sets of structure factors, to allow for different mean path lengths of the beam in the sample for symmetry-related reflections. Occupancy factors and all scattering lengths (Bacon, 1972) were kept fixed. The only irregularity in the refinement was that the coefficient b_{33} of the Mn atom became negative and had to be constrained to b_{22} of the same atom. Details of the refinement are given in Table 2. Difference Fourier maps computed at the end of the refinement from all reflections with F_{obs} corrected for extinction and F_{calc} showed no spurious peaks. The resultant atomic coordinates are given in Table 3.*

High-temperature phase (OHT)

Conditions for possible reflections ($0kl$, $k + l = 2n$ and $hk0$, $k = 2n$) give either a noncentrosymmetric (*Pn2b*, No. 30) or a centrosymmetric space group (*Pnmb*, No. 53). A non-standard cell setting, as listed in *International Tables for X-ray Crystallography* (1952), was used in order to keep the same notation of crystallographic axes for both phases and to allow direct comparison of both structures.

The phase transition is a distortive order–disorder transition of second order. This was established by ^{35}Cl and ^{2}H nuclear quadrupole resonance (NQR) spectroscopy and by birefringence measurements (Kind, Roos & Plesko, 1980). According to the Landau conditions (Landau, 1937) for second-order phase transitions, there must be a group–sub-group relation between the parent high-temperature (OHT) phase G_0 and the room-temperature (MRT) phase G_1 and the change of the crystal structure must correspond to a single irreducible representation of G_0, which cannot be the identity representation. In our case the size of the unit cell is unchanged and thus a change in the point group of order 2 must take place. Adding the new element $\{m_y|000\}$, found by NQR spectroscopy, to the symmetry elements of the MRT phase ($\{1|000\}\{2_z|0\frac{11}{22}\}\{\bar{1}|000\}\{m_z|0\frac{11}{22}\}$) results in the space group $P2/n\ 2/m\ 2_1/b$ (No. 53) (the elements $\{m_x|0\frac{11}{22}\}\{2_y|000\}$ and $\{2_x|0\frac{11}{22}\}$ are generated by multiplication of the symmetry elements). The change in the crystal, *i.e.* the frozen-in soft mode, transforms according to the Γ_3^+ representation of space group *Pnmb*. The general position in this space group is eightfold $\pm(x,y,z)$, $\pm(\bar{x},y,\bar{z})$, $\pm(x,\frac{1}{2}-y,\frac{1}{2}-z)$, $\pm(\bar{x},\frac{1}{2}-y,\frac{1}{2}+z)$.

The additional symmetry element, the mirror plane at $y = 0$ and $y = \frac{1}{2}$, constrains the in-plane Cl(1) atom to the special position $(x,\frac{1}{4},\frac{1}{4})$, the out-of-plane Cl(2) atom to the special position $(x,0,z)$ and causes the statistical disorder of the organic chain. Because the unit-cell dimensions in both phases are very close, the resultant fractional coordinates of the MRT phase were used (with the added constraints mentioned above) as starting parameters for the OHT phase.

The refinement of the OHT phase was performed in the same way as for the MRT phase. A good qualitative agreement between expected values of the scale factors and those from least-squares refinement indicates that the model of twinning and the assign-

* Lists of structure factors, anisotropic thermal parameters, the main axes of the thermal-vibration ellipsoids, a detailed list of interatomic bonds and valence angles for the OHT phase and Table 5 (least-squares planes, dihedral angles and other structural features) have been deposited with the British Library Lending Division as Supplementary Publication No. SUP 34992 (30 pp.). Copies may be obtained through The Executive Secretary, International Union of Crystallography, 5 Abbey Square, Chester CH1 2HU, England.

ment of the orienting reflections to the single-crystal individuals are correct.

In the course of the refinement, the ammonium H(3) atom had to be constrained to the mirror plane (in the special position $x,\frac{1}{2},z$) as its y value converged to 0·5 with b_{12} and b_{23} near zero (atoms located exactly on the mirror plane must have $b_{12} = b_{23} = 0$) and subsequently having diverged to 0·32 caused the whole refinement to stray. The aliphatic H(21) atom, on the other hand, also came close to the mirror plane (y = 0·427), but its temperature coefficients b_{12} and b_{23} were large, and therefore this atom was not constrained to the mirror plane. However, for all its parameters a large damping ('fudge' factors = 0·2) had to be applied in order to prevent an oscillation of their values.

Another interesting feature of the refinement was the presence of relatively small extinction effects. The same sample was used for the measurement of the MRT phase (with $\lambda = 1{\cdot}0308$ Å) and of the OHT phase (with $\lambda = 1{\cdot}2932$ Å) and although the measurement of the OHT phase was taken with a longer neutron wavelength, extinction attenuation factors were much smaller. The most affected reflection, 022, was reduced to 84 and 37% of its kinematic F^2_{obs} value for OHT and MRT phases respectively. Therefore, for the OHT phase the spread of mosaic blocks must be much larger and/or their size must be much smaller than for the MRT phase. This confirms the presence of the strain in the sample at high temperature mentioned in *Experimental.*

Description of the structures

The geometrical aspects of both structures are summarized in Tables 4 and 5* and in Figs. 2–6. For the sake of brevity, in the following text the numerical values for the MRT phase will be given in the 'numerator' and corresponding values for the OHT phase, separated by a || sign, will be in the 'denominator'. Estimated standard deviations (e.s.d.'s) in parentheses refer to the last significant figures.

* Table 5 has been deposited. See previous footnote.

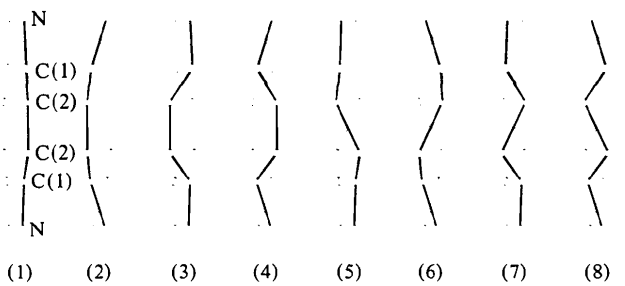

Fig. 2. Dynamically disordered atomic positions of the 1,4-butanediyldiammonium chain in the high-temperature phase and its possible instantaneous conformations. Hydrogen atoms are omitted for clarity; the mirror plane is perpendicular to the plane of the paper.

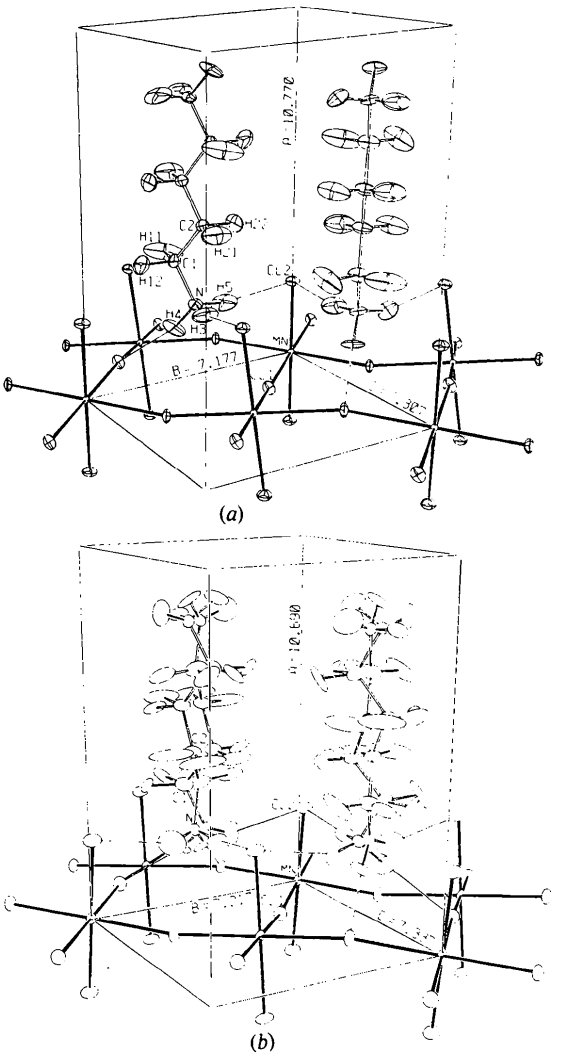

Fig. 3. Views (*ORTEP* II, Johnson, 1971) of the unit-cell contents showing the ordered and disordered organic chains below and above the phase-transition temperature. Hydrogen bonds are shown as light lines; thermal ellipsoids enclose: (*a*) 33% probability for the room-temperature (MRT) phase; (*b*) 15% probability for the high-temperature (OHT) phase; only conformation No. 4 of the chain is drawn.

The main feature of the structure is the presence of parallel two-dimensional perovskite-type $MnCl_4$ layers interleaved by layers of 1,4-butanediyldiammonium ions. Ammonium groups at both ends of the 1,4-butanediyl chains fit into cavities of the $MnCl_4$ layer (see Fig. 3) and $-N-H\cdots Cl$ hydrogen bonds thus bind 1,4-butanediyl chains to the neighbouring layers. Organic chains are extended along the longest a axis and exhibit large anisotropic thermal vibrations; the chains are ordered in the MRT phase but dynamically disordered in the OHT phase. R.m.s. amplitudes of

Table 4. *Selected interatomic distances* (Å) *and angles* (°)

The values were calculated with the program *ORFFE* (Busing, Martin & Levy, 1964) with a variance–covariance matrix and e.s.d.'s of cell parameters. Bond lengths C–H and N–H were corrected for riding motion, all other bond lengths for independent vibration of atoms. E.s.d.'s in parentheses refer to the last significant figures. The conformations 4 and 8 of the organic chain are marked by asterisks and daggers respectively.

Roman numerals as superscripts refer to the following equivalent positions which should be applied to the coordinates of the atom.

None	x,	y,	z	(xiii)	$1-x$,	$1-y$,	$-z$
(i)	$-x$,	$\frac{1}{2}-y$,	$-\frac{1}{2}+z$	(xiv)	$-x$,	y,	$-z$
(ii)	$-x$,	$\frac{1}{2}-y$,	$\frac{1}{2}+z$	(xv)	x,	$1-y$,	z
(iii)	x,	$\frac{1}{2}+y$,	$\frac{1}{2}-z$	(xvi)	$1-x$,	y,	$-z$
(iv)	$-x$,	$-y$,	$-z$	(xvii)	$-x$,	$\frac{3}{2}-y$,	$-\frac{1}{2}+z$
(v)	$-x$,	$1-y$,	$-z$	(xviii)	x,	$2-y$,	z
(vi)	x,	$1+y$,	z	(xix)	$-x$,	$1+y$,	$-z$
(vii)	$-x$,	$\frac{3}{2}-y$,	$\frac{1}{2}+z$	(xx)	x,	$-\frac{1}{2}+y$,	$\frac{1}{2}-z$
(viii)	x,	$\frac{3}{2}+y$,	$\frac{1}{2}-z$	(xxi)	x,	$-y$,	z
(ix)	$1-x$,	$1-y$,	$1-z$	(xxii)	x,	$-\frac{1}{2}+y$,	$\frac{3}{2}-z$
(x)	x,	y,	$1+z$	(xxiii)	$-x$,	$-y$,	$1-z$
(xi)	$1+x$,	y,	z	(xxiv)	x,	$-y$,	$1+z$
(xii)	x,	$\frac{1}{2}+y$,	$-\frac{1}{2}-z$	(xxv)	$-x$,	y,	$1-z$

	BDAMnCl$_4$, T = 295 K		BDAMnCl$_4$, T = 404 K	
	Uncorrected	Corrected	Uncorrected	Corrected
Metal–Cl$_4$ framework				
Mn–Cl(1)	2·595 (4)	2·608 (5)	2·582 (1)	2·615 (2)
Mn–Cl(2)	2·486 (4)	2·502 (4)	2·476 (4)	2·511 (5)
Mn–Cl(1^{i})	2·557 (4)	2·574 (5)	–	–
Cl(1)–Cl(1^{i})	3·693 (2)	3·704 (2)	–	–
Cl(1)–Cl(1^{xiv})	–	–	3·695 (2)	3·724 (2)
Cl(1)–Cl(2)	3·554 (5)	3·566 (5)	3·582 (6)	3·612 (6)
Cl(2)–Cl(1^{i})	3·532 (6)	3·545 (6)	–	–
Cl(2)–Cl(1^{iv})	–	–	3·573 (6)	3·605 (6)
Cl(1)–Mn–Cl(1^{i})	91·57 (3)		–	
Cl(1)–Mn–Cl(1^{xiv})	–		91·35 (4)	
Cl(2)–Mn–Cl(1)	88·7 (1)		90·2 (2)	
Cl(2)–Mn–Cl(1^{i})	88·9 (1)		–	
Mn–Cl(1)–Mn^{ii}	167·4 (1)		170·2 (2)	
Chlorine environment of N atom				
H-bonded chlorines				
N–Cl(2^{iii})	3·203 (7)	3·218 (7)	3·25 (2)	3·28 (2)
N–Cl(1^{v})	3·309 (7)	3·324 (7)	3·47 (3)	3·50 (3)
N–Cl(2)	3·373 (8)	3·384 (8)	3·42 (4)	3·45 (4)
Chlorines not H-bonded				
N–Cl(1^{i})	3·393 (8)	3·405 (8)	3·26 (3)	3·29 (3)
N–Cl(1)	3·360 (7)	3·373 (7)	3·40 (2)	3·42 (3)
N–Cl(1^{iii})	3·703 (8)	3·714 (7)	3·60 (2)	3·62 (2)
N–Cl(2^{vi})	3·824 (8)	3·834 (8)	3·81 (4)	3·83 (4)
N–Cl(2^{xii})	4·128 (7)	4·139 (7)	4·11 (2)	4·14 (2)
Hydrogen bonding				
N–H(3)	0·99 (2)	1·04 (2)	1·01 (3)	1·06 (3)
H(3)···Cl(2^{iii})	2·24 (1)	2·28 (1)	2·26 (2)	2·33 (2)
N ···Cl(2^{iii})	3·203 (7)	3·218 (7)	3·25 (2)	3·28 (2)
N–H(3)···Cl(2^{iii})	166·0 (1·3)		163·9 (1·7)	
N–H(4)	1·06 (1)	1·10 (2)	1·07 (5)	1·14 (6)
H(4)···Cl(1^{v})	2·28 (1)	2·32 (1)	2·41 (4)	2·47 (4)
N ···Cl(1^{v})	3·309 (7)	3·324 (7)	3·47 (3)	3·50 (3)
N–H(4)···Cl(1^{v})	165·0 (1·0)		172·9 (1·6)	
N–H(5)	1·03 (2)	1·10 (2)	0·87 (7)	0·96 (6)
H(5)···Cl(2)	2·39 (2)	2·43 (2)	2·64 (5)	2·70 (5)
N ···Cl(2)	3·373 (8)	3·384 (8)	3·42 (4)	3·45 (4)
N–H(5)···Cl(2)	160·3 (1·1)		150·7 (4·3)	
Possible H···Cl van der Waals contacts				
H(5)···Cl(1^{i})	2·84 (2)	2·87 (2)	2·83 (7)	2·89 (7)
N ···Cl(1^{i})	3·393 (8)	3·405 (8)	3·26 (3)	3·29 (3)
N–H(5)···Cl(1^{i})	114·3 (1·1)		112·9 (2·5)	
H(5)···Cl(1)	2·94 (2)	2·98 (2)	2·83 (5)	2·90 (4)
N ···Cl(1)	3·360 (7)	3·373 (7)	3·40 (2)	3·42 (3)
N–H(5)···Cl(1)	105·1 (1·0)		124·3 (4·4)	

Table 4 (*cont.*)

	BDAMnCl$_4$, T = 295 K		BDAMnCl$_4$, T = 404 K	
	Uncorrected	Corrected	Uncorrected	Corrected
Ammonium group				
N–H(3)	0·99 (2)	1·04 (2)	1·01 (3)	1·06 (3)
N–H(4)	1·06 (1)	1·10 (2)	1·07 (5)	1·14 (6)
N–H(5)	1·03 (2)	1·10 (2)	0·87 (7)	0·96 (6)
H(3)–H(4)	1·65 (2)	1·74 (2)	1·70 (3)	1·80 (4)
H(3)–H(5)	1·60 (2)	1·68 (3)	1·37 (7)	1·49 (6)
H(4)–H(5)	1·71 (2)	1·79 (2)	1·63 (6)	1·78 (5)
C(1)–N–H(3)	111·0 (0·9)		112·2 (2·7)	
C(1)–N–H(4)	111·5 (0·9)		100·6 (4·6)	
C(1)–N–H(5)	110·6 (0·9)		126·7 (6·6)	
H(4)–H(3)–H(5)	63·3 (1·0)		63·1 (2·4)	
H(5)–H(4)–H(3)	56·8 (1·1)		48·7 (2·8)	
H(3)–H(5)–H(4)	59·9 (0·9)		68·2 (2·6)	
H(3)–N–H(4)	108·1 (1·1)		109·2 (2·9)	
H(3)–N–H(5)	105·3 (1·5)		93·6 (3·2)	
H(4)–N–H(5)	110·0 (1·1)		114·1 (3·3)	
Organic chain N–(CH$_2$)$_4$–N				
N–C(1)	1·463 (8)	1·508 (7)	1·46 (5)	1·55 (2)
C(1)–C(2)	1·493 (8)	1·542 (8)	1·51 (6)	1·62 (3)
C(2)–C(2^{xiii})	1·43 (1)	1·52 (1)	1·60 (4)†	1·68 (3)†
C(2)–C(2^{xvi})	–	–	1·45 (4)*	1·54 (4)*
C(1)–H(11)	1·06 (2)	1·20 (2)	–	–
C(1)–H(11^{xv})	–	–	1·02 (5)	1·05 (4)
C(1)–H(12)	1·10 (2)	1·19 (2)	1·20 (1)	1·35 (10)
H(11)–H(12)	1·60 (3)	1·71 (2)	–	–
H(11^{xv})–H(12)	–	–	1·30 (6)	1·46 (6)
C(2)–H(21)	1·02 (2)	1·10 (3)	0·95 (5)	1·24 (11)
C(2)–H(22)	1·09 (2)	1·21 (3)	0·81 (10)	0·98 (8)
H(21)–H(22)	1·54 (2)	1·63 (2)	0·98 (17)	1·21 (10)
N–C(1)–C(2)	113·4 (0·5)		112·1 (5·9)	
C(1)–C(2)–C(2^{xiii})	113·2 (0·7)		104·3 (3·6)†	
C(1)–C(2)–C(2^{xvi})	–		117·1 (2·4)*	
N–C(1)–H(11)	111·6 (1·0)		–	
N–C(1)–H(11^{xv})	–		118·8 (2·2)	
N–C(1)–H(12)	106·9 (0·8)		113·7 (6·5)	
C(2)–C(1)–H(11)	112·9 (0·9)		–	
C(2)–C(1)–H(11^{xv})	–		120·7 (3·0)	
C(2)–C(1)–H(12)	114·6 (0·9)		113·2 (5·8)	
H(11)–C(1)–H(12)	96·0 (1·5)		–	
H(11^{xv})–C(1)–H(12)	–		71·9 (6·5)	
C(1)–C(2)–H(21)	112·6 (0·9)		117·7 (3·5)	
C(1)–C(2)–H(22)	111·7 (0·9)		120·4 (6·7)	
C(2^{xiii})–C(2)–H(21)	116·5 (1·1)		126·1 (4·9)†	
C(2^{xiii})–C(2)–H(22)	107·4 (1·0)		118·7 (2·3)†	
C(2^{xvi})–C(2)–H(21)	–		124·0 (3·0)*	
C(2^{xvi})–C(2)–H(22)	–		94·1 (2·2)*	
H(21)–C(2)–H(22)	93·7 (1·4)		67·0 (11·2)	

atomic vibrations are, on average, 1·5 times larger for all non-hydrogen atoms and 1·2 times larger for H atoms in the OHT phase than in the MRT phase.

(*a*) *Metal–tetrachloride framework*

The perovskite-type layer is ordered in both phases and consists of $MnCl_4$ planar ions (the planarity is imposed by Mn atoms occupying the centres of symmetry) so oriented that Mn and Cl(1) atoms form a puckered plane (see Fig. 5). The 'in-plane' Cl(1) atoms are displaced alternately below and above the plane defined by the Mn atoms [0·241 (3)‖0·220 (5) Å] and the corner-sharing $MnCl_6$ octahedra are alternately tilted backwards and forwards in the direction along the c axis. The layer is puckered two-dimensionally in the MRT phase; in the OHT phase, however, the mirror planes at $y = 0$ and $y = \frac{1}{2}$ constrain the Cl(1) and Cl(2) atoms to the special positions $(x,\frac{1}{4},\frac{1}{4})$ and $(x,0,z)$ respectively and therefore the less-pronounced puckering along the b axis of 179·4 (0·2)‖180·0 (0·0)° disappears, as does the small rotation of the $MnCl_6$

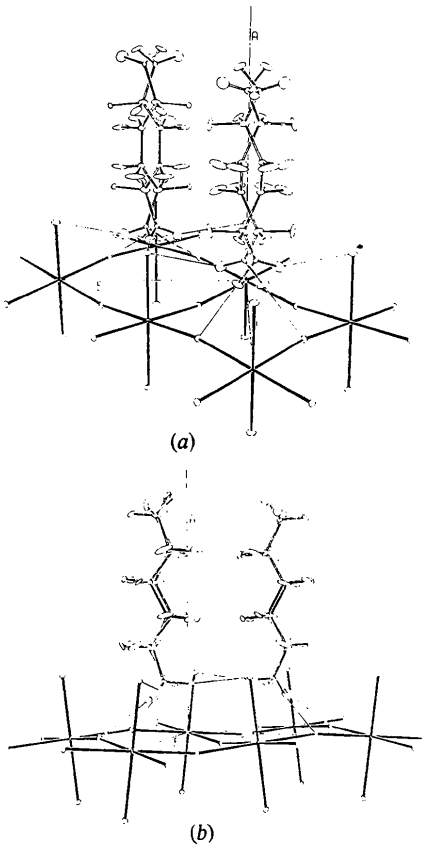

Fig. 4. The OHT phase of $BDAMnCl_4$ with thermal ellipsoids scaled to 3% probability (only conformation No. 4 of the chain is drawn). (*a*) View along the *c* axis. (*b*) View nearly along the *b* axis. Note that the puckering of the $MnCl_4$ layer is in the direction of the *c* axis only.

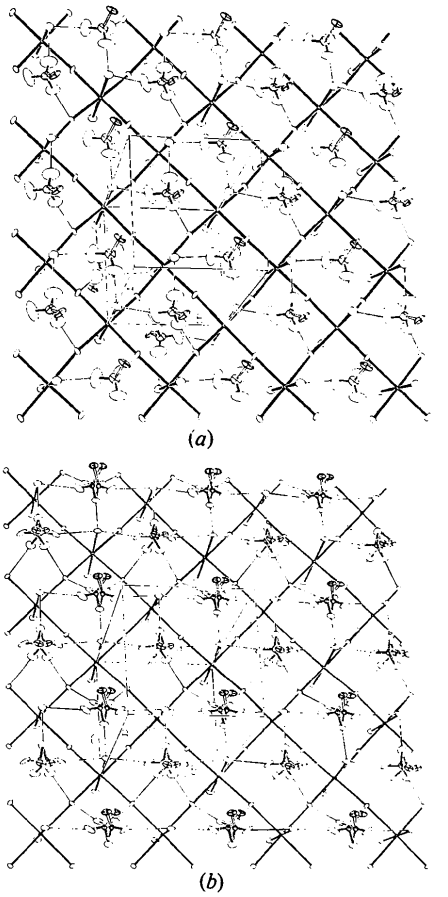

Fig. 5. Hydrogen-bonding scheme of $BDAMnCl_4$. Only the $-C-NH_3$ groups of the organic chains and the metal–tetrachloride framework are drawn. (*a*) The MRT phase; thermal ellipsoids are scaled to 50% probability. (*b*) The OHT phase; thermal ellipsoids are drawn to 10% probability only. Note that the H(3) atoms are in non-disordered positions on the mirror planes $y = 0$ and $y = \frac{1}{2}$.

octahedra about the *a* axis. The puckering along the *c* axis [164·6 (0·2)‖166·4 (0·4)°] changes in the same way as the magnitude of the valence angle Mn–Cl(1)–Mn [167·4 (1)‖170·2 (2)°].

The environment of the Mn atom differs qualitatively in both phases. In the MRT phase the neighbouring ions are approximately at right angles to each other and an 'in-plane' Cl(1) atom from a neighbouring ion thus comes close to the Mn atom giving rise to the octahedral coordination around it [with the in-plane distances Mn–Cl(1) = 2·608 (5) and 2·574 (5) Å and 'out-of-plane' distance Mn–Cl(2) = 2·502 (4) Å]. In the OHT phase, however, the $MnCl_6$ octahedron is even more regular, as its 'own' Cl(1) atom and its 'neighbour's' Cl(1) atom are at the same distance from the Mn atom [two equal 'in-plane' distances of 2·615 (2) Å] and thus $MnCl_4$ ions lose their individuality. The 'out-of-plane' distance is 2·511 (5) Å. The Mn–Cl(2) bond is nearly perpendicular to the *bc* plane [82·2 (1)‖83·4 (2)°]; the valence angle Cl(1)–Mn–Cl(2) is 88·7 (1)‖90·2 (2)°.

Bond distances and angles (Tables 4 and 5) are consistent with those of the $MnCl_6$ octahedra in similar compounds, *e.g.* $EDAMnCl_4$ (Tichý *et al.*, 1978), $[CH_3(CH_2)_2NH_3]_2MnCl_4$ (Peterson & Willett, 1972), $(CH_3CH_2NH_3)_2MnCl_4$ (Depmeier, 1976), $NH_3(CH_2)_3NH_3MnCl_4$ (Willett & Riedel, 1975), and $(CH_3NH_3)_2MnCl_4$ (Heger, Mullen & Knorr, 1976).

(*b*) *Organic chain* NH_3–$(CH_2)_4$–NH_3

In the MRT phase the skeleton N–C–C–C–C–N is very nearly planar; the exact planarity of the –C(1)–C(2)–C(2)–C(1)– segment is imposed by the centre of symmetry at the middle of the C(2)–C(2) bond; the torsion angle of the N–C(1) bond from this planar segment is 2·6 (1·1)°. The ammonium H(4) atom lies nearest to the N–C–C–C–C–N plane and continues its zigzag line. The other two ammonium H atoms, H(3) and H(5), lie nearly symmetrically on both

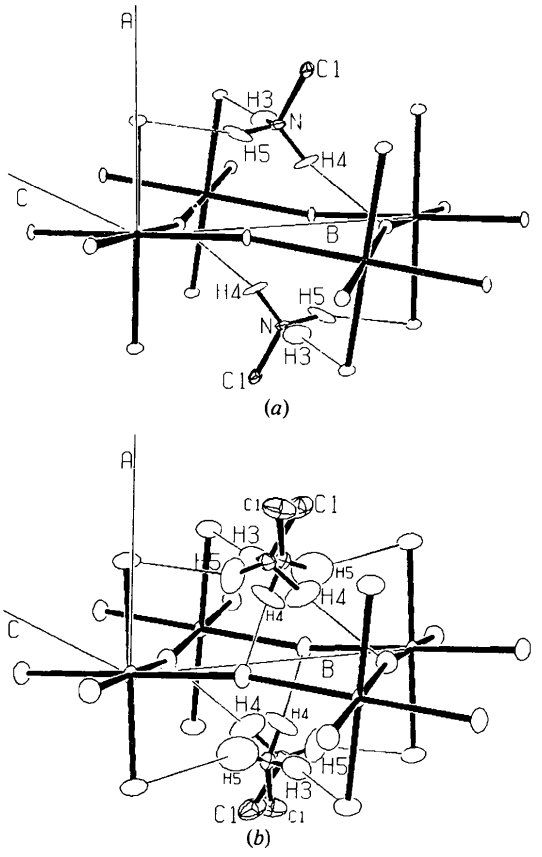

Fig. 6. Embedding of the $-NH_3$ group inside the cavity in the $MnCl_4$ layer lined by eight Cl atoms. Ellipsoids of thermal vibrations include 20% probability. (*a*) The MRT phase. (*b*) The OHT phase.

sides of the plane. The organic chains are completely isolated from one another as there are no contacts shorter than 3·0 Å between neighbouring chains (including CH_2 hydrogen atoms) and there is enough space between chains to make their large anisotropic thermal vibrations (even at room temperature) physically reasonable (see Fig. 3). Uncorrected values of C–N and C–C bonds are in good agreement with bond lengths for $EDACuCl_4$ and $EDAMnCl_4$ (Tichý *et al.*, 1978) and for $NH_3(CH_2)_3NH_3MCl_4$ (M = Mn, Fe) (Willett & Riedel, 1975). The bond lengths and angles summarized in Table 4 and the dihedral angles between the planes defined by different segments of the organic ion (see Table 5) have no unexpected value and indicate that there is no deformation of the 1,4-butanediyldiammonium ions due to their insertion between $MnCl_4$ sheets.

In the OHT phase the whole organic ion [with the exception of the H(3) atom] is dynamically disordered, spending equal time in both positions related by the mirror plane. This is shown schematically in Fig. 2, with the H atoms omitted for clarity. The diffraction experiment thus yields two positions for each atom of the chain with population parameters = ½, but it does not give any information about the way in which the disordered atomic positions are linked by the chemical bonds, *i.e.* about the conformation of the disordered chain. There are eight possible instantaneous conformations of the chain (see Fig. 2), representing different modes of chain vibration. Solid evidence about the conformation could be supplied by spectroscopic or inelastic scattering data. Unfortunately, no such data are available and therefore we can only say that some conformations are more probable than others.

To arrive at a probable instantaneous conformation of the chain, we used standard bond lengths (*International Tables for X-ray Crystallography*, 1962) for C–H = 1·06–1·12, N–H = 1·01–1·13, C–N = 1·479 ± 5 and aliphatic C–C = 1·541 ± 3 Å. It turned out that conformation No. 4 has the best agreement of bond lengths with the above standard values. On the other hand, from symmetry requirements of the phase transition (see *Discussion*) it is evident that conformation No. 8 must be present in the OHT phase. The two conformations differ only in the C(2)–C(2) bond; for a more detailed analysis see *Discussion*. Bond lengths and angles of the MRT phase and those of conformations 4 and 8 of the OHT phase are summarized in Table 4; a more comprehensive table of distances and angles between positions of the disordered organic chain has been deposited.

(*c*) *Hydrogen-bonding scheme*

Organic chains are linked to the metal–halogen framework by hydrogen bonds involving the ammonium groups which enter into the cavities of the $MnCl_4$ layer lined by eight Cl atoms. These Cl atoms act as acceptors for ammonium H atoms to build weak $-N-H\cdots Cl$ bonds.

In the MRT phase the hydrogen bonding is essentially the same as in $EDAMnCl_4$. Although ammonium H atoms exhibit hindered rotation about the C(1)–N bond (Kammer, 1976*a*,*b*), their rest positions are non-disordered (verified by a difference Fourier synthesis) between the N atom and two out-of-plane Cl(2) atoms and one in-plane Cl(1) atom. The lengths of the hydrogen bonds and their $N-H\cdots Cl$ angles are 2·282 (12), 2·428 (15) and 2·316 (13) Å and 166·0 (1·3), 160·3 (1·1) and 165·0 (1·0)°, respectively. As in $EDAMnCl_4$ there are no $H\cdots Cl$ contacts shorter than 2·8 Å and, as the hydrogen bonds are fairly straight, one may conclude that the $H\cdots Cl$ bonds are pure hydrogen bonds with no van der Waals $H\cdots Cl$ contacts (Koetzle, Lehmann, Verbist & Hamilton, 1972).

In the OHT phase the positions of the atoms of the ammonium group are dynamically disordered [with the exception of the H(3) atom, which sits in the mirror

plane] but its instantaneous conformation can very well be identified by analysing the interatomic distances and valence angles of the atomic positions of the disordered ammonium group. A position corresponding to the MRT phase is denoted in Fig. 6(*b*) by larger lettering than a position corresponding to its mirror image. Also, the instantaneous bonding system is the same as in the MRT phase, *i.e.* two H atoms, H(3) and H(5), to out-of-plane Cl(2) atoms, one H(4) atom to the in-plane Cl(1) atom. The non-split position of the H(3) atom corresponds to the shortest (and strongest) hydrogen bond of 2·282 (12)‖2·328 (17) Å. The longest hydrogen bond [H(5)–Cl(2) 2·699 (52) Å] in the OHT phase is also least straight [150·7 (4·3)°] and it seems that the effect of the van der Waals attraction of the two next shortest H(5)···Cl contacts [2·873 (12)‖2·888 (67) and 2·975 (17)‖2·895 (43) Å] is more pronounced than in the MRT phase. When the ammonium group jumps from one of the two stable positions to the other, the rest position of the H(3) atom remains stable while the rest position of the in-plane-Cl(1)-bonded H(4) atom jumps to the rest position of the out-of-plane-Cl(2)-bonded H(5) atom and *vice versa*.

Fig. 5(*a*) illustrates how adjacent ammonium groups in the MRT phase are hydrogen-bonded to the metal–halogen framework. Each out-of-plane Cl(2) atom is bonded to two H atoms belonging to two neighbouring ammonium groups, while each in-plane Cl(1) atom is linked to only one H atom, H(4). The bond Cl(1)···H(4) contributes to the lifting of the Cl(1) atom and thus to the tilting of the $MnCl_6$ octahedron. The sequence of hydrogen bonds ···H(5^a)–N^a–H(3^a)···Cl(2^I)···H(5^b)–N^b–H(3^b)···Cl(2^{II})··· runs across the crystal in a zigzag line parallel to the *b* axis and the pair of bonds H(3^a)···Cl(2^I)···H(5^b) tilts the $MnCl_6$ octahedron in the same direction as it is already tilted by the lifting-up effect of the H(4)···Cl(1) bond.

In the OHT phase (see Fig. 5*b*) the mirror plane $\{m_y|000\}$ located at $y = 0$ and $y = \frac{1}{2}$ symmetrizes the above-mentioned zigzag lines into a system of flat ridges and sharp ditches made from hydrogen bonds, with the effect that the in-plane Cl(1) atom is now linked to two H(4) atoms, 50% of the time to each. The out-of-plane Cl(2) atom is linked 50% of the time to the H(5) of one ammonium group and 50% of the time to the H(5) atom of the next ammonium group along the *b* axis. At the same time, the Cl(2) atom is linked 100% of the time to the H(3) atom, and this explains why the H(3)···Cl(2) bond is the strongest in the OHT phase. For possible reasons for the bond H(3)···Cl(2) being also the strongest hydrogen bond in the MRT phase, see *Discussion*.

Table 6. *Dimensions* (Å) *and orientations of the* $MnCl_6$ *octahedra in* $EDAMnCl_4$ *and* $BDAMnCl_4$

	Bond below or above *bc* plane	$EDAMnCl_4$	$BDAMnCl_4$ $T = 295$ K	$BDAMnCl_4$ $T = 404$ K
Mn–Cl(1)	below	2·579 (3)	2·608 (5)	2·615 (2)
Mn–Cl(2)	above	2·508 (4)	2·502 (4)	2·511 (5)
Mn–$Cl(1^i)$	above	2·600 (3)	2·574 (5)	2·615 (2)

Discussion

In both phases large anisotropic thermal vibrations of organic chains are possible because of a complete lack of contact between neighbouring chains. Although the ammonium group $-NH_3$ exhibits hindered rotation (as in $EDAMnCl_4$, Kammer, 1976*a*,*b*) in both phases, the amplitudes of thermal vibrations of ammonium H atoms are smaller than those of H atoms in the CH_2 groups.

For the dynamically disordered organic chain, conformation No. 4 in Fig. 2 is the best from the crystallographic point of view of bond lengths and angles. Some objections can be raised against this conformation. The first and obvious objection is that it is energetically unstable, as the torsion angle about the C(2)–C(2) bond is 52 ± 10° and therefore near to the potential-energy maximum. The maximum, however, is rather low; for the butane chain in the gaseous state it is 14·6 kJ mol^{-1} only and the energy necessary for the 1,4-butanediyldiammonium chain to adopt conformation No. 4 can well be supplied by thermal motion in the crystal.

For further objections we also have to discuss the seven remaining conformational modes of the chains according to Fig. 2. Modes 1, 2, 3, 4 transform according to the X_4^+ representation of the space group *Pnmb*, *i.e.* if such a mode should become soft, the space group of the low-temperature phase would be *Pnab* (No. 60) with $Z = 4$. This would imply a doubling of the orthorhombic unit cell in the **a** direction, *i.e.* perpendicular to the layers. Modes 5, 6, 7, 8 transform according to the Γ_3^+ representation of the space group *Pnmb*, *i.e.* they transform like the soft mode of our phase transition *Pnmb* → $P2_1/b$. The only mode containing the observed low-temperature structure with an almost planar chain is mode No. 8. It can thus safely be assumed that this mode must be present in the high-temperature phase. This does not, of course, imply that the other seven modes do not exist.

To arrive at the most probable instantaneous conformations of the chain, one has to consider the bond lengths within the chain as well as the energy needed for the deformation of the chain according to Fig. 2. The energy is given by the number of torsions of the chain. Such a torsion can be defined as a departure from the relative 180° orientation of successive CH_2 groups. Since the torsion angles computed from the

resulting atomic positions are all either ~0 or ~60°, there would also have to be a contribution of energy from the C–N bond if its torsion angle were 60°. A torsion of the $-CH_2-NH_3$ group of about 60° leads from the *trans* configuration to the eclipsed configuration. According to this definition we have five torsions for mode No. 1, three torsions for Nos. 2 and 3, one for No. 4, four for No. 5, two for Nos. 6 and 7 and none for No. 8.

For the bond lengths within the chain we assumed the standard values. Although conformation No. 4 in Fig. 2 is the best from a crystallographic point of view, we have already seen that this conformation does not transform according to the soft mode, but since it contains only one torsion it is energetically reasonable to assume its presence as well. On the other hand, conformation No. 8 cannot be the only one present in the OHT phase because the interatomic distance C(2)–C(2) [with expected standard value 1·541 (3) Å] would be too long [1·600 (35) Å uncorrected for thermal motion and 1·678 (30) Å corrected for independent vibration of the atoms]. Even if one takes into account that the e.s.d.'s based on least-squares refinement may be underestimated for the sample which was both twinned and disordered, the C–C values of 1·541 and 1·678 Å are not easy to reconcile.

A speculative superposition of conformations 4 and 8 fulfils the requirements of the Landau theory (see, for example, Blinc & Žekš, 1974) for second-order phase transitions and allows for a reasonable C(2)–C(2) bond length in conformation No. 8. Such a superposition requires an additional splitting of the atoms of the organic chain. The splitting assumed to be predominantly in the direction of the *b* axis can be very small* (~0·1 Å) to achieve an acceptable C(2)–C(2) distance and is supported by the large amplitudes of vibrations of the C(1), C(2) and N atoms in the direction of the *b* axis.

It is therefore very probable that conformations 4 and 8 are mainly present in the OHT phase at the temperature under which the measurement was performed, whereas the other six conformations are less probable for energetical reasons.

Despite the similarity of the unit-cell parameters *b*, *c* and γ and of the puckering of the metal–halogen framework of $EDAMnCl_4$ and $BDAMnCl_4$, there is an important difference in the orientation of the $MnCl_6$ octahedron in the framework, namely that it is turned by ~90° about the Mn–Cl(2) bond. As can be seen from Table 6, the lengths of all Mn–Cl bonds are identical within experimental error for both structures, but the lengths of the Mn–Cl(1) and Mn–Cl(1^i) bonds are interchanged. This explains the difference in the unit-cell parameters *b* and *c*, which one would otherwise expect to be exactly the same because of the complete isolation of one organic chain from another. This 90° turn of the octahedra may correspond to another important difference in both structures, namely to the difference in the hydrogen-bonding scheme (see Table 7). The shortest (and strongest) hydrogen bond in $EDAMnCl_4$ (and also in $EDACuCl_4$) is the in-plane bond Cl(1^v)···H(4)–N while in both phases of $BDAMnCl_4$ the strongest is the out-of-plane bond Cl(2^{iii})···H(3)–N. It is not clear which one of these two differences is the primary cause. Purely phenomenologically, it may be said that in $EDAMnCl_4$ the Cl(1^v)–H(4) bond is the strongest because of its uniqueness of being the link between only one H(4) atom and only one in-plane Cl(1) atom, while the other two out-of-plane Cl(2) atoms are each linked to two H(3) and H(5) atoms. Analogically, it may be pointed out that in the OHT phase of $BDAMnCl_4$ the bond H(3)–Cl(2^{iii}) is so strong because the Cl(2^{iii}) atom is 100% of the time (the time spent by ammonium H atoms on hindered rotation ≪ time spent in the resting position) linked to a H atom occupying the only non-disordered position H(3), while the other two bonds are weaker as they are occupied 50% of the time only, and for the MRT phase this state is one of the 'frozen' states of the OHT phase.

Table 7. *Lengths* (Å) *and angles* (°) *of the hydrogen bonds in* $EDAMnCl_4$ *and* $BDAMnCl_4$

	$EDAMnCl_4$	$BDAMnCl_4$ $T = 295$ K	$BDAMnCl_4$ $T = 404$ K
N–H(3)···Cl(2^{iii})	2·300 (11)	2·282 (12)	2·328 (17)
	165·9 (8)	166·0 (1·3)	163·9 (1·7)
N–H(4)···Cl(1^v)	2·286 (12)	2·316 (13)	2·469 (38)
	177·7 (9)	165·0 (1·0)	172·9 (1·6)
N–H(5)–Cl(2)	2·376 (12)	2·428 (15)	2·699 (52)
	162·3 (8)	160·3 (1·1)	150·7 (4·3)

However, the most plausible explanation seems to lie in a higher rigidity of the ethylenediammonium chain. The N–C–C–N skeleton is constrained to a plane (by the centre of symmetry at the middle of the C–C bond) and this leaves to the ammonium $-NH_3$ group only one degree of freedom, namely the angle of rotation about the C–N bond. For the H atoms of the $-NH_3$ group so constrained, the energy of hydrogen bonding reaches its minimum when metal–Cl_6 octahedra are oriented in a certain way, *i.e.* when the longest in-plane metal–Cl distance is the metal–Cl(1^i) bond.

In the 1,4-butanediyldiammonium chain, the N–C(1) bond is not constrained by the centre of

* The atomic position of the C(2) atom split into two positions 0·097 Å apart in the **b** direction {y[C(2)] = 0·4530 (24) and y' = 0·4664} yields for conformation No. 8 an acceptable bond length of C(2)–C(2) = 1·528 Å (uncorrected for thermal motion). The shift amounts to 5·5 times the e.s.d. of the y[C(2)] coordinate and to $\frac{1}{3}$ of the r.m.s. amplitude of the thermal-motion ellipsoid in the direction of the *b* axis. [The r.m.s. displacements in the principal axes of the ellipsoid of thermal vibrations of the C(2) atom are 0·167, 0·254 and 0·290 Å and are approximately in the directions of the crystallographic axes *a*, *c* and *b* respecitvely.]

symmetry at the middle of the C(2)–C(2) bond to the plane of the planar segment C(1)–C(2)–C(2)–C(1). The ammonium group thus has two degrees of freedom, one of rotation about the C(1)–N bond (as in the EDA chain) and, in addition, one degree of freedom of the deviation of the C(1)–N bond from the plane of the planar segment C(1)–C(2)–C(2)–C(1), *i.e.* the torsion angle about the C(1)–C(2) bond, which is 2·6 (1·1)° for the BDA chain in the MRT phase. This additional degree of freedom apparently permits the finding of a minimum for the hydrogen-bonding energy, which is lower when the metal–Cl_6 octahedra are turned by ~90° about the metal–Cl(2) bond, *i.e.* when the longest in-plane distance is the metal–Cl(1) bond.

The above speculations are supported by the fact that the puckering along the *c* axis in $EDAMnCl_4$ [162·4 (0·2)°] is larger than in the MRT phase of $BDAMnCl_4$ [164·6 (0·2)°], which indicates that the strain imposed on the metal–tetrachloride framework is larger for the EDA chain than for the BDA chain. The lack of structural phase transition in $EDAMnCl_4$ and $EDACuCl_4$ between room temperature and the decomposition temperature suggests that the ethylenediammonium chain is too strongly bonded to the metal–Cl_4 matrix to allow for a dynamical disorder of the chains.

In the OHT phase, the disappearance of the slight puckering along the *b* axis of the metal–halogen framework is caused by the mirror symmetry of five hydrogen bonds of the dynamically disordered ammonium group. The degree of puckering [166·4 (0·4)°] of the layer in the OHT phase is smaller than in the MRT phase [164·6 (0·2)°]; this is caused by the overall weakening of the hydrogen bonding, the dynamical disorder and the larger amplitudes of thermal vibrations of the ammonium H atoms.

Conclusions

The structures of both phases were refined with H atoms and with anisotropic temperature factors for all atoms; the success of the refinement of the OHT phase is an ultimate verification that the assignment of orienting reflections to the single-crystal individuals (Tichý & Beneš, 1979) was correct.

In contrast to twinned $EDACuCl_4$ and $EDAMnCl_4$, where almost 100% of the reflections were measured, we were able to separate only 80 and 70% of the reflections from their reflection satellites for the quadruplicated MRT phase and the triplicated OHT phase of $BDAMnCl_4$, respectively. Also a higher percentage of separated reflections was affected by a partial overlap with their satellites, resulting in a worse agreement in unweighted $R(F) \sim 0{\cdot}17$ [for a study on twins $R(F) \sim 0{\cdot}09$] at almost the same agreement in weighted $R_w(F) \sim 0{\cdot}07$ [for twins $R_w(F) = 0{\cdot}04$ and 0·08]. These two facts indicate that the method used for data measurement and treatment has a limit of about six or seven single-crystal individuals present in a measured sample.

We have shown the existence of dynamical disorder of the 1,4-butanediyldiammonium chain in the OHT phase which is 'frozen-in' in the MRT phase. The best explanation for our results is the superposition of the soft Γ_3^+ mode with a low-energy zone-boundary mode X_4^+ in the parent phase *Pnmb*. Below the second-order phase transition the soft mode freezes-in, whereas the X_4^+ mode dies out since it does not correspond to a stable configuration of the chain. Concerning the striking difference of the $MnCl_6$ octahedra orientations between the room-temperature structures of $EDAMnCl_4$ and $BDAMnCl_4$ we can give only speculative arguments. To answer this question a detailed study of similar compounds with longer chains would have to be undertaken.

We thank Drs W. Bührer, Institut für Reaktortechnik, ETH, Zürich, J. Roos, Physics Institute, University of Zürich, M. Dobler, Department of Organic Chemistry, ETH, Zürich, Professor R. D. Willett, Department of Chemistry, Washington State University, for useful discussions and comments. Further, we thank Dr K. Peng, Swiss Federal Institute for Reactor Research, for taking powder diffractograms for an accurate unit-cell determination, Dr W. Petter, Institute of Crystallography, ETH, Zürich, for allowing one of us to use his Weissenberg goniometer and Mr M. Zazzeri, Laboratory of Solid-State Physics, ETH, Zürich, for cutting the sample used in this neutron study. Our thanks are also due to Professor W. Hälg for his steady interest in the present work.

References

AREND, H., HUBER, W., MISCHGOFSKY, F. H. & RICHTER-VAN LEEUWEN, G. K. (1978). *J. Cryst. Growth*, **43**, 213–223.

AREND, H., TICHÝ, K., BABERSCHKE, K. & RYS, F. (1976). *Solid State Commun.* **18**, 999–1003.

BACON, G. E. (1972). *Acta Cryst.* A**28**, 357–358.

BENEŠ, J. & TICHY, K. (1975). *Acta Cryst.* A**31**, S295.

BLINC, R. & ŽEKŠ, B. (1974). *Soft Modes in Ferroelectrics and Antiferroelectrics*, edited by E. P. WOHLFARTH, p. 67. Amsterdam, Oxford: North-Holland, Elsevier.

BUSING, W. R., MARTIN, K. O. & LEVY, H. A. (1962). *ORFLS*. Report ORNL-TM-305. Oak Ridge National Laboratory, Tennessee.

BUSING, W. R., MARTIN, K. O. & LEVY, H. A. (1964). *ORFFE*. Report ORNL-TM-306. Oak Ridge National Laboratory, Tennessee.

DEPMEIER, W. (1976). *Acta Cryst.* B**32**, 303–305.

HEGER, G., MULLEN, D. & KNORR, K. (1976). *Phys. Status Solidi A*, **35**, 627–637.

International Tables for X-ray Crystallography (1952). Vol. I, pp. 546–548. Birmingham: Kynoch Press.

International Tables for X-ray Crystallography (1962). Vol. III, pp. 270–276. Birmingham: Kynoch Press.
JOHNSON, C. K. (1971). *ORTEP* II. Report ORNL-3794, revised. Oak Ridge National Laboratory, Tennessee.
KAMMER, H. (1976*a*). *Helv. Phys. Acta*, **49**, 726–727.
KAMMER, H. (1976*b*). Proc. 19th Congr. Ampère, Heidelberg, pp. 487–490.
KIND, R., ROOS, J. & PLESKO, S. (1980). In preparation.
KOETZLE, T. F., LEHMANN, M. S., VERBIST, J. J. & HAMILTON, W. C. (1972). *Acta Cryst.* B**28**, 3207–3214.
LANDAU, L. D. (1937). *Phys. Z. Sowjetunion*, **11**, 26.
PETERSON, E. R. & WILLETT, R. D. (1972). *J. Chem. Phys.* **56**(5), 1879–1882.
TICHÝ, K. (1970). *Acta Cryst.* A**26**, 295–296.
TICHÝ, K. & BENEŠ, J. (1977). *Helv. Phys. Acta*, **50**, 459–466.
TICHÝ, K. & BENEŠ, J. (1979). *J. Appl. Cryst.* **12**, 10–14.
TICHÝ, K., BENEŠ, J., HÄLG, W. & AREND, H. (1978). *Acta Cryst.* B**34**, 2970–2981.
WALPEN, P. (1976). Diploma work, Institute for Crystallography, ETH, Zürich.
WILLETT, R. D. & RIEDEL, E. F. (1975). *Chem. Phys.* **8**, 112–122.
ZACHARIASEN, W. H. (1967). *Acta Cryst.* **23**, 558–564.

Acta Cryst. (1980). B**36**, 1367–1371

Xanthate and Dithiocarbamate Complexes of Group II*b* Elements, and an Interesting Relationship Between Two Mercury(II) Ethylxanthate* Phases

BY CHUNG CHIEH AND KELLY J. MOYNIHAN

Guelph Waterloo Centre for Graduate Work in Chemistry, Department of Chemistry, University of Waterloo, Waterloo, Ontario, Canada N2L 3G1

(*Received* 31 *August* 1979; *accepted* 20 *February* 1980)

Abstract

Crystals of mercury(II) ethylxanthate, $[Hg(C_3H_5OS_2)_2]$, obtained from acetone are monoclinic with $a = 9{\cdot}300$ (2), $b = 6{\cdot}693$ (2), $c = 19{\cdot}585$ (9) Å, $\beta = 100{\cdot}94$ (3)°, space group $P2_1/c$, $Z = 4$. The structure was determined by the heavy-atom method from 2111 diffractometer-measured reflections. The crystal consists of mica-like two-dimensional sheets formed by mutual bridging of Hg^{II} and ethylxanthate ions. The Hg^{II} ion is bonded to four S atoms with Hg–S distances of 2·417 (4), 2·421 (4), 2·789 (4) and 2·854 (4) Å. The coordination geometry is a very distorted tetrahedron with a large and a small S–Hg–S angle of 147·7 (1) and 84·3 (1)°, respectively. The sheets are stacked parallel to the (001) plane; alternate layers are related by a center of symmetry. In contrast, the same compound crystallized from CCl_4 belongs to $P2_1$. The structures within the layers are the same but the packing arrangements of the sheets are different in the two crystals.

Introduction

Both dithiocarbamates and xanthates are useful industrial chemicals with a common functional group $-C(=S)S^-$ (Rao, 1971). In 1978, Japan granted a patent for using an aqueous solution containing 0·01–0·25% xanthate and sodium tellurate to remove mercury from industrial waste gas at 313 K. These S-containing materials offer great potential for the industrial-waste treatment required in environmental protection.

We have reported several crystal structures of Hg^{II} complexes of diethyldithiocarbamate (dtc) in our studies of interactions between *N*,*N*,*N*′,*N*′-tetraethylthiuram disulfide (TETD) and mercurials (Chieh, 1978; Chieh & Leung, 1976). In these structures, the $-C(=S)S^-$ group was found to be a unidentate, bridging or chelating ligand. As part of this continuing study, mercury(II) ethylxanthate was synthesized and its crystal structure studied.

A structure of mercury(II) ethylxanthate has been reported previously (Watanabe & Hagihara, 1972; Watanabe, 1977). Their cell constants and space group differ from ours, yet the two sets of data are related (see below) in an interesting way. Our study has confirmed that the two phases from acetone and CCl_4 belong to $P2_1/c$ and $P2_1$ respectively.

In this paper, we are directing our attention to the close structural relationships among M(xanthate)$_2$ compounds, where M = Zn, Cd, and Hg. Factors leading to the differences between the structures of the xanthates and dithiocarbamates of these metals are explored.

* IUPAC name: mercury bis(*O*-ethyl dithiocarbonate).

0567-7408/80/061367-05$01.00